SEMARAK ILMU PUBLISHING

Journal of Advanced Research in Applied Mechanics

Journal homepage:
https://semarakilmu.com.my/journals/index.php/appl_mech/index
ISSN: 2289-7895

Identification of Power Quality Disturbances in Electrical Distribution System using Fast Fourier Transforms and Super Learner Ensembles

Supakan Janthong[1,2], Pornchai Phukpattaranont[1,*]

[1] Department of Electrical and Biomedical Engineering, Faculty of Engineering, Prince of Songkla University, Songkhla 90110, Thailand
[2] Provincial Electricity Authority, Bangkok 10900, Thailand

ARTICLE INFO

Article history:
Received 20 June 2024
Received in revised form 1 August 2024
Accepted 9 August 2024
Available online 30 August 2024

Keywords:
Power quality disturbances; machine learning techniques; detection and classification; super learner ensembles

ABSTRACT

Currently, the use of non-linear loads and equipment, as well as renewable energy sources injected into the power system, tends to increase. As a result, the waveform of the electrical signal changes, and distortion occurs in the distribution system, which affects the quality and reliability of the electrical system. Importantly, sometimes this leads to malfunctions in protection equipment. This paper presents the algorithm for power quality disturbance (PQD) identification in electrical distribution systems, which involves three main steps: (1) Generating simulated waveforms using a signal processing approach; (2) extracting features using the Fast Fourier Transforms (FFT) technique; and (3) identifying the type of PQD using Super Learner Ensembles (SLE), which employs cross-validation to assess the performance of multiple machine learning models. Subsequently, the model's efficiency is verified and tested using data from electronic energy meters installed in the distribution system of the Provincial Electricity Authority (PEA). The accuracy resulting from synthetic and experimental data sets is 99.90% and 99.69%, respectively. The results indicate that the model performs well in identifying power quality disturbances and achieves high accuracy.

1. Introduction

Power quality disturbances (PQDs) refer to deviations or variations in the standard electrical characteristics of the power supply, which have the potential to negatively impact the functionality of electrical and electronic equipment [1]. The origins of these disturbances can be diverse, and their severity varies depending on the type of equipment and the sensitivity of the connected loads. Additionally, the integration of renewable energy sources, such as solar photovoltaic systems and wind turbines, into the electrical grid is becoming increasingly significant, which can introduce various interference problems concerning power quality for utilities [2]. These issues arise due to the intermittent and variable nature of renewable energy sources and their interactions with the existing power grid.

* *Corresponding author.*
E-mail address: pornchai.p@psu.ac.th

https://doi.org/10.37934/aram.124.1.3960

The examination of causes and effects contributing to PQD reveals a multitude of sources. PQD can arise from various factors, including faults within the electricity grid, disruptions caused by the integration of renewable energy sources, and distortion and flow back into the distribution system due to customer load behavior. The specific details pertaining to single PQD instances are summarized and presented in Table 1.

As shown in Table 1, some of the potential PQD issues that may arise include voltage fluctuations, voltage sags and swells, harmonics, transients, and power interruptions. Voltage fluctuations manifest as variations in voltage levels due to changes in load demand. Voltage sags and swells are brief reductions or increases in voltage levels that can be caused by faults or sudden load changes. Harmonics, on the other hand, result from non-linear loads, such as variable speed drives and specific lighting systems, introducing additional frequencies into the system. Transients are characterized by short-duration voltage spikes or surges arising from lightning strikes, switching operations, or other rapid changes in the electrical system. Lastly, power interruptions encompass unplanned power outages, equipment failures, or disruptions in electricity supply.

The Provincial Electricity Authority (PEA) is entrusted with the responsibility of electricity distribution in various provinces of Thailand [3]. As with any power distribution utility, the PEA may encounter PQD problems within its electrical distribution network [4]. To ensure the reliability and stability of the electrical system and the connected equipment, regular power quality monitoring and analysis are of paramount importance. Therefore, this research project proposes to develop a machine learning system for the detection and classification of power quality disturbances. By proactively identifying and mitigating potential PQD issues, adverse consequences and disruptions can be mitigated before they escalate into significant damage or disturbances to the electrical network.

Table 1
Causes and effects of a single PQD instance

Causes	Effects	PQD
Renewable energy integration: the intermittent nature of sources	Data loss and corruption Power system instability	Voltage fluctuations Frequency variations Power imbalances
Faults and equipment failures: short circuits or equipment failures within the distribution network	Equipment damage and malfunction Electrical fires	Voltage sags Interruptions Transient/Impulse/Spike
Load variations: rapid changes in load demand due to industrial processes, commercial activities, or weather conditions	Flickering lights Voltage fluctuations and unbalanced currents	Voltage swells Flicker
Harmonics: non-linear loads, such as electronic devices and lighting with power electronics	Customer dissatisfaction Leading to voltage distortions Increased heating in transformers and conductors	Harmonics
Poor power factor: low power factor due to reactive power consumption by certain loads	Reduced efficiency Leading to increased losses	Oscillatory

2. Related Work

Power quality disturbances (PQDs) have been categorized according to the IEEE standard 1159-2019 [5]. The presence of voltage and current distortions has led to ongoing research in the field of electric power quality disturbances, focusing on their detection and classification. These disturbances

can be divided into two primary groups based on their waveform-time statistical characteristics [6]: stationary waveform disturbances, wherein the waveform's nature remains unchanged over time, and non-stationary disturbances, where the waveform's nature changes with time. Both groups are crucial for researchers to comprehend the underlying phenomena.

The development of an automatic power quality classifier for identifying PQD involves a two-step approach [7]. Firstly, modern signal processing techniques are employed, which encompass segmentation and feature extraction in the pre-processing step. For instance, during segmentation, the non-stationary component is isolated from the waveform components. The root mean square values of the distorted and pure signals are compared to identify the disturbed segment [8]. Feature extraction involves extracting relevant information from the raw signal to facilitate more effective processing. This process transforms the data into a new format, making it easier to extract pertinent and critical data. Numerous signal processing techniques are employed in feature extraction.

The Fourier transform stands as a fundamental signal processing tool employed in the characterization of steady-state phenomena. To address and alleviate the limitations stemming from slow constraint dynamics and sensitivity, Liu *et al.,* introduced the generalized discrete Fourier transform [9]. While the Fourier transform serves as a frequency transform, the short-time Fourier transform (STFT) is utilized to explore the time-frequency domain.

The wavelet transform (WT) offers insights into both the frequency components of a signal and its time resolution. Through a process of decomposition, a given signal is split into multiple signals with varying resolutions, which proves especially beneficial for analyzing non-stationary signals [10]. The decomposition is achieved through the application of discrete wavelet transforms and second-generation wavelet transforms across four hierarchical levels. Comparative evaluations reveal that the second-generation wavelet transform outperforms the discrete wavelet transform in terms of speed and efficiency [11].

The S transform (ST) capitalizes on the multi-resolution analysis of WT and effectively incorporates frequency variables akin to STFT, which reside between STFT and WT in the signal processing domain [12]. For the non-stationary voltage flicker, separating the flicker signal from the voltage signal poses a computational challenge due to its high complexity [13]. In light of this, Shamachurn *et al.,* conducted a comparative study between ST and a modified version called the modified S transform (MST), employing diverse classifiers to assess the obtained results. The results demonstrate that MST, as a modified variant of ST, exhibits superior accuracy when compared to conventional ST [14]. Moreover, MST serves as a valuable tool for evaluating power quality in utility systems integrated with renewable energy sources [15].

In the Hilbert Huang transform (HHT), the energy signal is initially subjected to empirical mode decomposition to obtain intrinsic mode functions, which are subsequently analyzed through the Hilbert transform to determine the signal's frequency and amplitude characteristics [16]. Additionally, an improved version of the ST was integrated into the HHT, leading to the proposal of the Iterative Hilbert-Huang Transform. This enhancement effectively addresses the challenge of detecting neighboring frequency components and amplitudes within waveforms obtained from PQD events [17]. In the work presented by Sahani and Dash [18], real-time PQD detection and classification were accomplished using HHT combined with a weighted bidirectional extreme machine learning approach. Similarly, Hemapriya *et al.,* [19] employed HHT in conjunction with support vector machines (SVM) for classification purposes. In both instances, HHT played a crucial role in extracting relevant features prior to input into the respective learning models.

The subsequent step in identifying PQD involves the adoption of artificial intelligence techniques encompassing classification and recognition. To address the classification of multiple classes of PQD, the directed acyclic graph SVM approach was implemented [20]. For receiving and classifying PQD

signals, an event-driven A/D converter was utilized in conjunction with SVM and Naive Bayes classifiers [21], which is similar to a previous study [22] that employed the decision tree algorithm. The latter yielded superior results compared to the other two techniques. Zhu *et al.,* proposed the utilization of a Global Deep-Shuffle Convolutional Neural Network (GSCNN) to enhance performance and reduce the number of parameters [23]. However, it should be noted that the GSCNN was notably deep and complex and did not involve the extraction of features. For real-time PQD monitoring systems, fuzzy logic and criterion-based classifiers were integrated [24]. Unfortunately, the paper did not provide a comprehensive description of the various classifier parameters utilized in this context.

Despite the successful outcomes of numerous studies in the field, there are still certain gaps that warrant improvement in the real-world application of PQD identification. These gaps are highlighted as follows:

i. Firstly, a significant portion of current research concentrates on combinations of feature extractors, which can introduce complexities in the extraction process. As a consequence, more time and processing resources are consumed.
ii. Secondly, the focus of research primarily revolves around classifier design, leading to a deficiency in comprehensive investigations concerning eigenvalue extraction. This oversight results in the neglect of relationships between key features, leading to the inclusion of more information than necessary.
iii. Thirdly, a majority of research has opted for machine learning techniques to classify PQD, yet the appropriateness and rationale for the adoption of specific machine learning methods have not been thoroughly evaluated. Given that each type of machine learning algorithm possesses distinct functionalities, it is essential to consider their suitability for distinct PQD classification tasks.
iv. Fourthly, the generation of PQD data using mathematical models tends to be somewhat idealistic, even though these models are based on the IEEE standard 1159-2019. Consequently, the performance of the model in terms of learning and classification might be superior to that achieved with real-world data, which is influenced by various factors beyond the mathematical models' considerations.

This study presents an efficient algorithm for identifying single PQD in electrical distribution systems, employing fast Fourier transform (FFT) and super learner ensemble (SLE). The key contributions of this research can be summarized as follows:

i. Firstly, in order to streamline the extraction process and enhance processing speed, FFT is utilized as the fundamental technique for transforming signals into the frequency domain.
ii. Secondly, to optimize model performance, SLE is adopted, which employs cross-validation to evaluate the efficacy of multiple machine learning models. This approach proves to be superior in prediction and achieving overall better model performance compared to other participatory models.
iii. Thirdly, in addition to assess the trained and validated model using generated data, a real dataset obtained from electronic meters (Elec-meters) installed in the Provincial Electricity Authority (PEA) is utilized to evaluate the model's performance.
iv. Fourthly, to ensure minimal complexity and resource consumption, the generated model takes the form of a feed-forward architecture, which enables rapid and accurate processing.

The rest of this paper is organized as follows: Section 3 describes the generation of PQD datasets and the proposed methodology. Section 4 presents the results compared with previous studies, the discussion, and the limitations. Finally, Section 5 summarizes the research and gives future work prospects.

3. Materials and Methods

In this section, the generation of PQD data sets consisting of synthetic and experimental data sets is described. Then, the proposed methodology consisting of signal preprocessing, feature extraction, and classification is given. Finally, performance evaluation methods are provided. The details of each subsection are as follows:

3.1 PQD Datasets

There are two PQD data sets used in this paper, namely synthetic and experimental data sets. Details of each data set are given as follows:

3.1.1 Synthetic dataset

In the analysis of PQD to accurately represent real-time signals, the utilization of mathematical equations becomes necessary for generating synthetic PQD signals. It is imperative for the generated synthetic signal to encompass all the properties of the real-time signal and closely match it in all aspects. The present study encompasses eight types of single disturbances, namely sag, swell, oscillatory, flicker, harmonics, interruption, transient/impulse/spike, and notch. The mathematical model of each single disturbance and its corresponding parametric configuration are provided in Table 2, with the parameters being based on the IEEE standard 1159-2019 [25]. Examples of the eight generated signals are shown in Figure 1. The period of complete disturbance consists of other disturbance events.

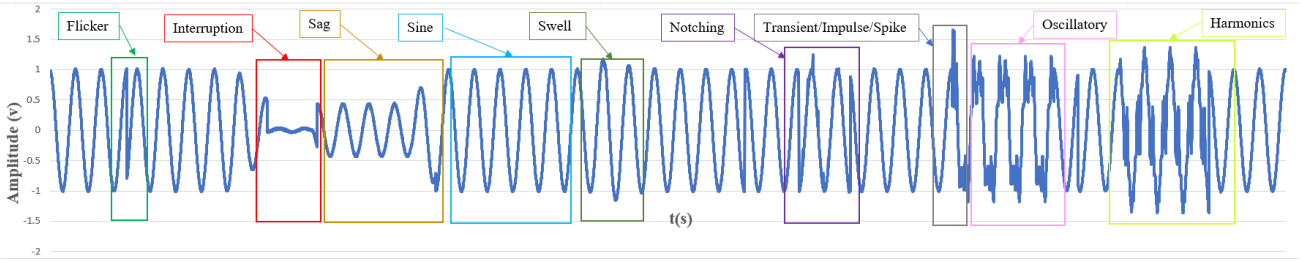

Fig. 1. Waveform of voltage signal with disturbance events

Table 2 presents a mathematical framework delineating PQD in accordance with IEEE 1159-2019 guidelines, wherein nine distinct configurations are formulated to synthesize data using MATLAB. The synthesized signal employed for simulation purposes is generated in a stochastic manner, adhering to parameters as stipulated in Table 3. These parameters encompass characteristics such as disturbance onset time, duration, and amplitude. The synthesis process yielded a total of 2,700 disturbance signal instances, each characterized by specific attributes, including a sampling rate of 12,800 Hz, a fundamental frequency of 50 Hz, and a frame duration of 100 ms were used. Then, a parameter value from Table 2 was randomly selected. For example, in the case of sag or swell, a number in the given range shown in the last column of Table 2 was randomly chosen. A windowing function of type Rectangular Window which is a simple window where all data points within the

window have the same weight. The simulation encompassed a duration spanning five cycles. All simulations were conducted on an Intel Core i7-12700H 2.30 GHz CPU accompanied by 16 GB of RAM.

Table 2
Mathematical model and parameter setting of PQD

No.	PQDs	Equations	Parameters
1	Pure	$v(t) = A\sin(\omega t)$	$A = 1(pu), \omega = 2\pi f\ rad/s, f = 50\ Hz$
2	Sag	$v(t) = A(1-\alpha(u(t-t_1)-u(t-t_2)))\sin(\omega t)$	$0.1 \le \alpha \le 0.8, T \le (t_2-t_1) \le 9T$
3	Swell	$v(t) = A(1+\alpha(u(t-t_1)-u(t-t_2)))\sin(\omega t)$	$0.1 \le \alpha \le 0.8, T \le (t_2-t_1) \le 9T$
4	Oscillatory	$v(t) = A[\sin(\omega t) + \beta e^{-(t-t_1)/\tau}u(t-t_1)$ $-u(t-t_2)\sin(2\pi f_n t)]$	$0.1 \le \beta \le 0.8, 0.5T \le (t_2-t_1) \le 3T$ $8ms \le \tau \le 30ms, 300 \le f_n \le 900Hz$
5	Flicker	$v(t) = A[1+\lambda\sin(\kappa\omega t)]\sin(\omega t)$	$0.1 \le \lambda \le 0.2, 5 \le \kappa \le 10$
6	Harmonics	$v(t) = A[\alpha_1\sin(\omega t) + \alpha_3\sin(3\omega t) +$ $\alpha_5\sin(5\omega t) + \alpha_7\sin(7\omega t)]$	$0.1 \le \alpha_3, \alpha_5, \alpha_7 \le 0.15, \alpha_1 = 1$
7	Interruption	$v(t) = A(1-\alpha(u(t-t_1)-u(t-t_2)))\sin(\omega t)$	$0.9 \le \alpha \le 1, T \le (t_2-t_1) \le 9T$
8	Transient/ Impulse/ Spike	$v(t) = \sin(\omega t) + \alpha_t \exp(-\frac{t-t_1}{\tau})(u(t-t_1)-u(t-t_2))$	$3 \le \alpha_t \le 4, 0.5T \le (t_2-t_1) \le 3T$ $8ms \le \tau \le 30ms$
9	Notching	$v(t) = \sin(\omega t) - sign(\sin(\omega t))$ $\sum_{n=0}^{9}(K \times [u\{t-(t_1-0.02n)\}-u\{t-(t_2-0.02n)\}])$	$0.1 \le K \le 0.4, 0 \le t_1, t_2 \le 0.5T,$ $0.01T \le t_2 - t_1 \le 0.5T$

Table 3
Simulated characteristics of PQD

Simulation Events	Type of PQD	Time duration	Voltage magnitude
Switching of large loads (ON many air conditioners)	Sag	> 0.5cycles	0.9–0.1pu
Switching of large loads (OFF many air conditioners)	Swell	> 0.5cycles	1.8–1.1pu
Circuit breaker operation (At MDB)	Interruption	> 0.5cycles	< 0.1pu
Non-linear loads (ON) (LED, UPS, computers, printers)	Harmonics	> 50ms	0.2–0.0pu
Load switching (At MDB)	Oscillatory	5< t < 50ms	8–0pu
Motor starting (Pump motor)	Flicker	Steady state	-
Switching of heavy load	Notching	Steady state	-
Capacitor bank switching	Transients	> 50ms	-

We can observe an illustrative PQD signal in Table 4. The table is divided into two sections: on the left, we have the original amplitude-time (s) waveform, and on the right, the data from the left side is transformed into the frequency domain using FFT (Power Spectrum). In this representation, the sample spacing is measured in seconds, while the frequency unit is given in cycles per second. The transformed outcomes provide an alternate perspective on the data's transformation. The table encompasses nine distinct waveform categories: pure, sag, swell, oscillatory, flicker, harmonics,

interruption, transient, and notching. The distinct pattern that emerges is more noticeable when compared to the waveform in the time domain.

Table 4
Visualization between raw data and FFT

	Raw data	FFT
Pure	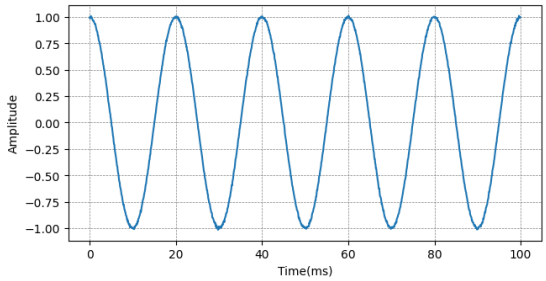	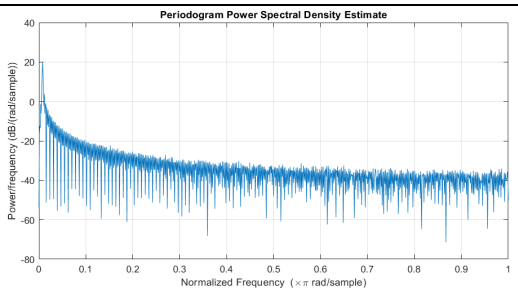
Sag	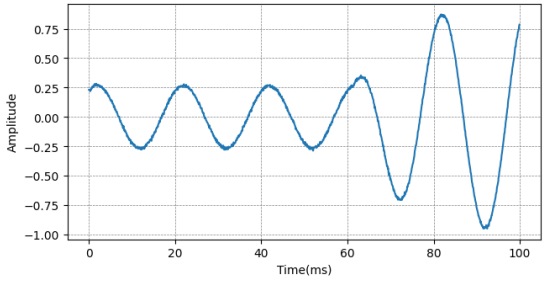	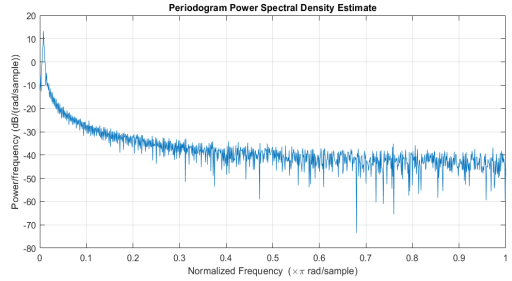
Swell	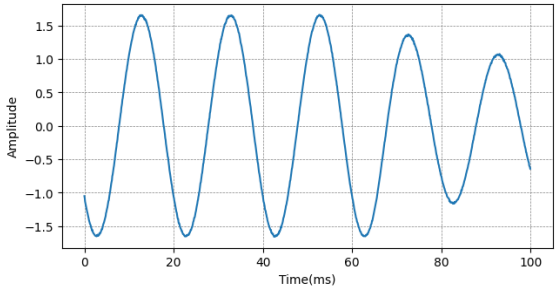	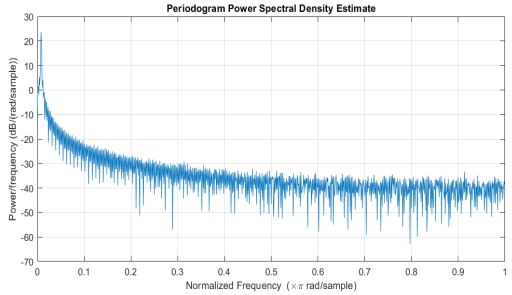
Oscillatory	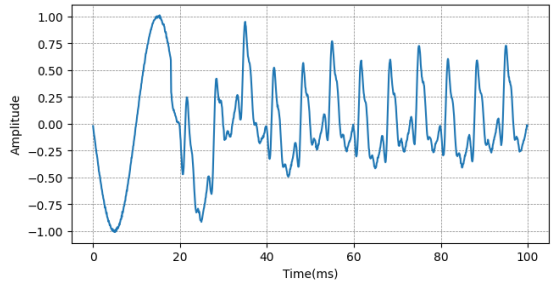	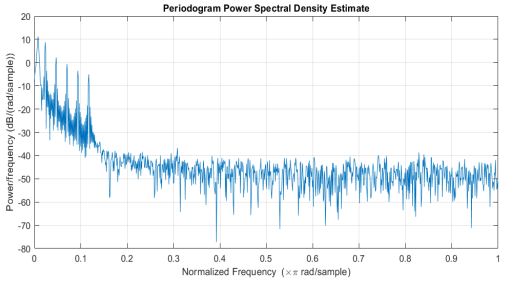
Flicker	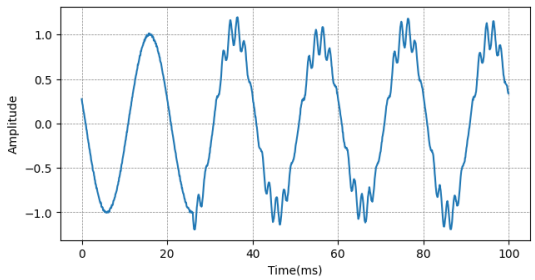	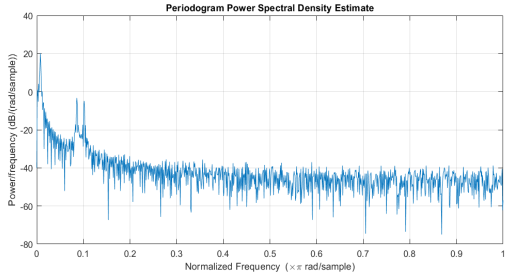

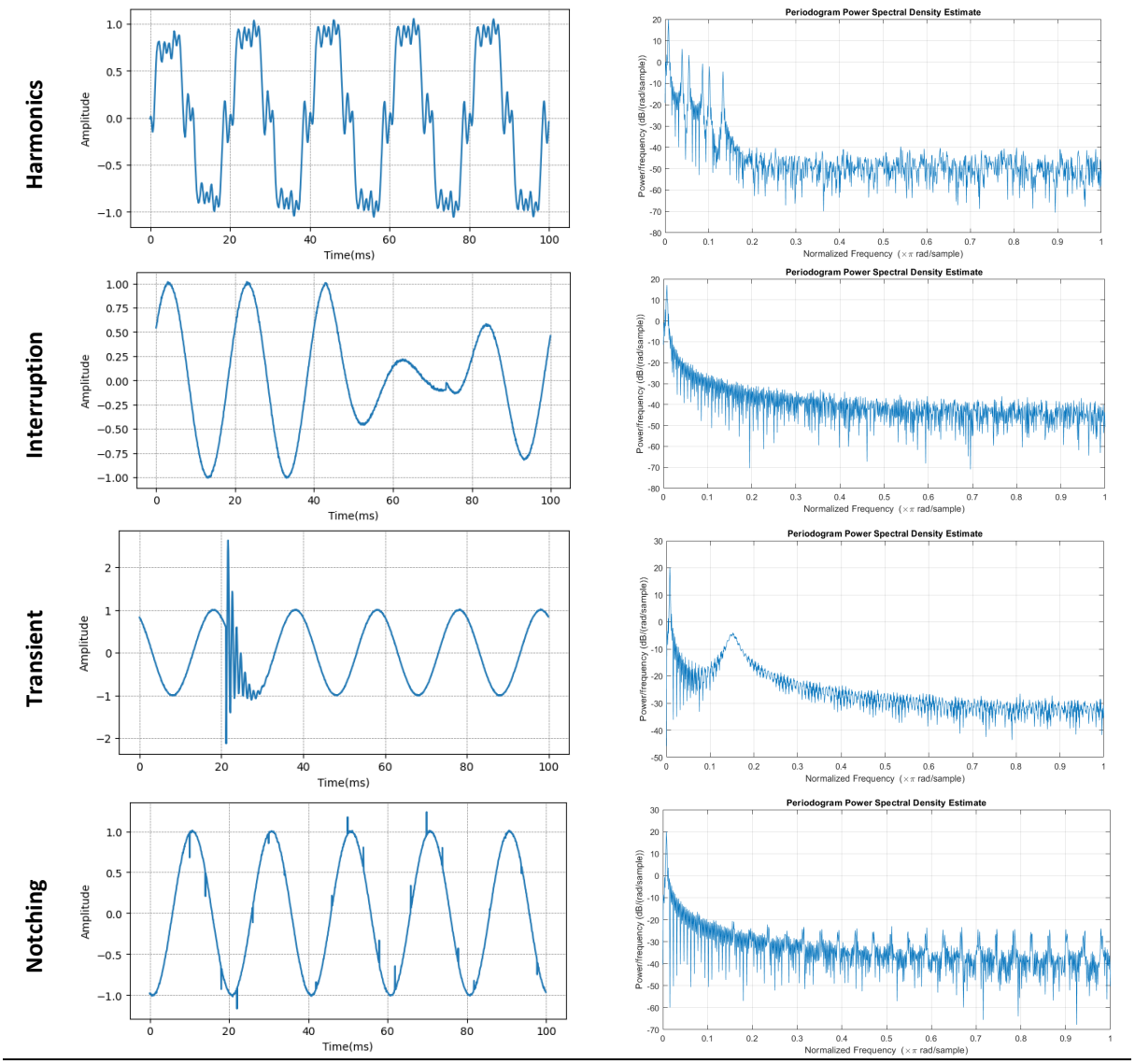

3.1.2 Experimental dataset

Within the distribution system of PEA, a variety of meter types have been installed, including electromechanical meters (kilowatt-hour meters), electronic meters (Elec-meters), automatic meter reading, and smart meters [28]. Each meter type possesses distinct functionalities and data recording capabilities. Kilowatt-hour meters lack the ability to record historical data, while Elec-meters can store Bluetooth reading data for up to 90 days. On the other hand, automatic meter reading and smart meters, integrated into advanced metering infrastructure systems, enable the storage of load profiles in a database for backup purposes.

Experimental or real data acquisition in this study is acquired from Elec-meters, as they are widely deployed across all areas and cater to various customer types, including residential houses, businesses, and industries. Due to the inherent limitations of Elec-meters in terms of online communication, data collection necessitates on-field visits to the meter installations. In the experiment, a 3-phase, 4-wire Elec-meter (EDMI product meter, GENIUS model) was used to collect real data. The complete details and specifications of the electronic meter are: a voltage rating of 3x220/380 volts, a current rating of 5 (6) amps, class 0.5, double protection, a constant value per

1000 cycles/kilowatt-hour, and 1,000 cycles/kilovar-hour. The main components inside the meter include:

i. A current sensor, which is a sensor installed on the power supply line to measure the amount of current flowing through it;
ii. A voltage sensor, which is a sensor connected to a wiring harness to measure the voltage of the power supply;
iii. A processor, which is a microprocessor used to calculate the amount of electricity used and store the information in the meter's memory;
iv. A display, which is a digital display that shows the amount of electricity and other information such as the current time and the rate of electricity consumption;
v. A communication module, which is a module that allows the meter to communicate. Here, communication is possible via the Port RS-232 module and optical probes.

Figure 2 shows the process involves retrieving load profile data and capturing all recorded information on events, which is then subjected to analysis. The real data acquired from Elec-Meters used for testing the model was taken from the simulated event shown in Table 3. A record of the voltage was collected at a sampling rate of 12,800 Hz, a fundamental frequency of 50 Hz with a frame duration of 100 ms and a duration of 5 cycles. The meter installed at the office was connected to a laptop to keep records. Then, the events were simulated using the office's existing load. This simulation strategy ensured the correspondence of each PQD pattern with a distinct time interval.

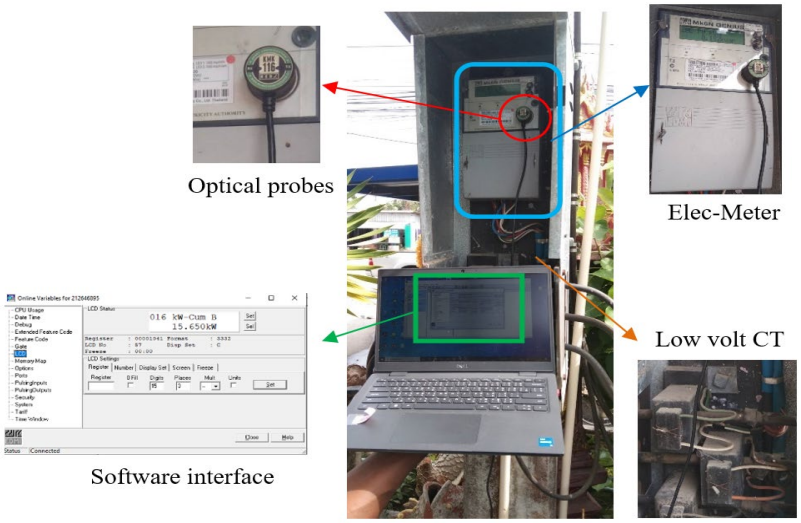

Fig. 2. Load profile retrieval process

The information was gathered from meters installed at the PEA office. To facilitate data retrieval, an optical probe is interfaced with a laptop computer, employing the EziView program specifically designed for the Elec-meters. Communication is established through the connection of the optical probe to a USB port. Throughout the experimental procedure, voltage and current measurements were acquired, as illustrated in Figure 3. Phase voltage (230V to 220V) was recorded, and a segment of the current was subjected to conversion through a 250/5 A current transformer (CT) in instances where meter-detected distortions were encountered (Figure 4).

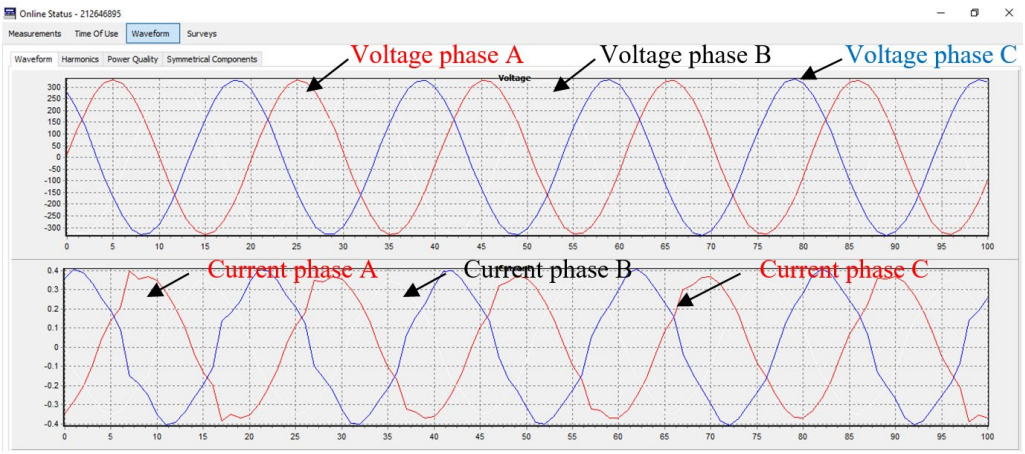

Fig. 3. Voltage and current signals read from Elec-meter

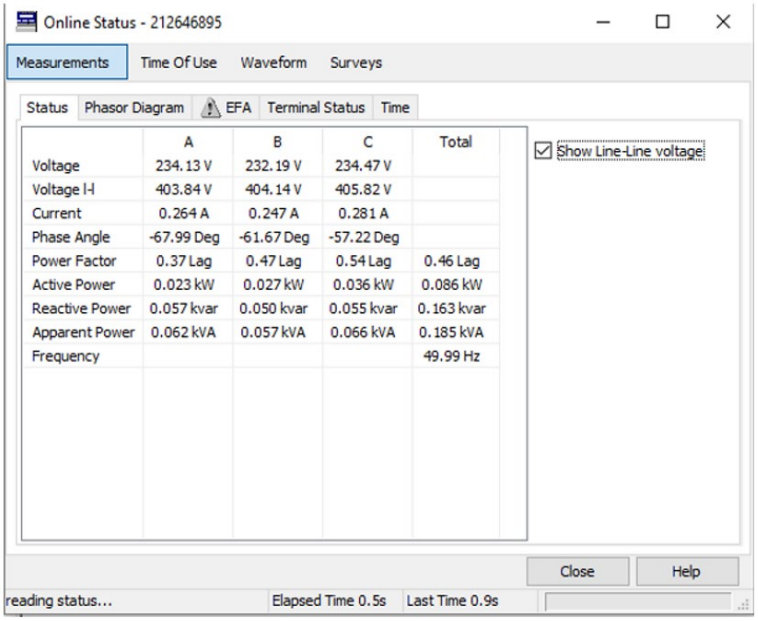

	A	B	C	Total
Voltage	234.13 V	232.19 V	234.47 V	
Voltage l-l	403.84 V	404.14 V	405.82 V	
Current	0.264 A	0.247 A	0.281 A	
Phase Angle	-67.99 Deg	-61.67 Deg	-57.22 Deg	
Power Factor	0.37 Lag	0.47 Lag	0.54 Lag	0.46 Lag
Active Power	0.023 kW	0.027 kW	0.036 kW	0.086 kW
Reactive Power	0.057 kvar	0.050 kvar	0.055 kvar	0.163 kvar
Apparent Power	0.062 kVA	0.057 kVA	0.066 kVA	0.185 kVA
Frequency				49.99 Hz

Fig. 4. Parameters measured by Elec-meters

The display window in Figure 3 showed three sets of voltage and current waveforms, where red represented phase A, white represented phase B, and blue represented phase C. Volts/Div was set to 50, which meant that the scale in each channel was a voltage of 50 volts. Amps/Div was set to 2, which meant that the scale in each channel was a current of 2 amps. Cycles were set at five. The capture section consisted of Continuous and Remove the DC Offset modes. The waveform image was updated all the time in Continuous mode. Remove DC Offset was used to remove the DC offset in order to view the value of alternating current only. In the experiment, data were recorded via Memory Map by selecting Load Survey mode. All the data was exported as text files and then imported to Excel for filtering. In this experiment, only voltage and current values were chosen to be analyzed.

3.2 Proposed Methodology

The machine learning system for the detection and classification of PQD events in this study consists of three steps: signal preprocessing, feature extraction, and classification. The details of each step are as follows:

3.2.1 Signal preprocessing

The synthesized data will be normalized according to Eq. (1)- Eq. (3) because machine learning models are sensitive to numerical data. Bias can occur if the data ranges are very different.

Standardization; $$X_{std}^{n} = \frac{x_i - \mu_t}{\sigma_t} \quad (1)$$

Mean; $$\mu_t = \frac{1}{N}\sum_{i=1}^{N}(x_i) \quad (2)$$

Standard deviation; $$\sigma_t = \sqrt{\frac{1}{N}\sum_{i=1}^{N}(x_i - \mu_t)^2} \quad (3)$$

where: x_i is the sample of all values obtained from signal generation. μ_t is the mean and σ_t is standard deviation in one cycle t, respectively.

3.2.2 Feature extraction

The FFT feature is extracted from the normalized data described in the last section. FFT is a widely used algorithm for efficiently computing the discrete Fourier transform and its inverse, the inverse discrete Fourier transform [26]. In the context of PQD, FFT is employed to analyse the frequency components of voltage and current waveforms to identify and characterize various disturbances, such as sag, swell, interruption, harmonics, interharmonics, flicker, etc. The discrete Fourier transform equation for a discrete time-domain signal of samples is given by:

$$X(k) = \sum_{n=1}^{N-1}[X_{std}^{n} e^{(-j2\pi kn/N)}] \quad (4)$$

where $X(k)$ is the complex-valued frequency-domain representation at bin *k*, and *j* is the imaginary unit. To obtain the magnitude spectrum (amplitude) of the frequency components, we use:

$$\left|X(k)\right| = \sqrt{(\mathrm{Re}[X(k)]^2 + \mathrm{Im}[X(k)]^2)} \quad (5)$$

where $\mathrm{Re}[X(k)]$ and $\mathrm{Im}[X(k)]$ are the real and imaginary parts of $X(k)$, respectively. The phase angle spectrum can be calculated as:

$$\varphi(\mathrm{k}) = \tan^{-1}\left(\mathrm{Im}\left[X(k)\right], \mathrm{Re}\left[X(k)\right]\right) \quad (6)$$

In the context of power quality disturbances, analysts often use the magnitude spectrum to identify the presence and magnitude of harmonics, interharmonics, and other disturbances. The phase angle spectrum is useful for determining the phase relationships between different harmonic components. By analysing the FFT results, PQD experts can pinpoint the frequencies and magnitudes

of disturbances in the electrical system, enabling them to take appropriate corrective actions to mitigate PQD issues and ensure a more reliable and efficient power supply.

For achieving optimal attributes, the FFT method was employed to extract the pertinent data, as shown in Algorithm 1. This approach incorporates a windowing function to mitigate spectral leakage, thereby enhancing the overall fidelity of the outcome. In our experiment, we use a rectangular window, which is a simple window where all data points within the window have the same weight. The calculation of corresponding frequency values was accomplished for the discrete FFT bins. Notably, the frequency resolution (designated as delta_f) was derived by dividing the sampling rate by the total number of samples (N). The obtained results were visualized through the depiction of spectral magnitude using a graphical representation. Subsequent analysis of frequency components enabled the identification of PQD. The process of FFT feature extraction was facilitated using the scipy.fft library [30].

Algorithm 1: Feature Extraction Using FFT for PQD signals

```
Input:        V(t) signal waveform
Parameters:   Sampling_rate = 12,800
Output:       fft_result, frequencies
              # Define FFT
                def fft_analysis(signal, sampling_rate):
              # Apply a windowing function
                    windowed_signal = apply_window(signal)
              # Compute FFT
                    fft_result = np.fft.fft(signal)
              # Compute Frequency
                 N = len(signal)
                 delta_f = sampling_rate / N
                 frequencies = np.arange(0, N) * delta_f
                 return fft_result, frequencies
              # Plotting magnitude spectrum
                Plot(frequencies, np.abs(fft_result))
```

3.2.3 Classification

The FFT features from nine PQD signals are classified using a super learner ensemble (SLE). The SLE is an ensemble learning method used to improve the accuracy and performance of predictive models by combining multiple base learners [27]. In the context of PQD, the SLE can be applied to analyse and predict the occurrence and characteristics of PQD events based on various features extracted from voltage and current waveforms. The SLE is constructed by combining the predictions of multiple base learners, typically represented as follows:

$$\hat{y}_{SLE} = \sum_{i=1}^{n} W_i * \hat{y}_i \tag{7}$$

where $\hat{y}_{SLE}$ is the super learner ensemble's prediction, $\hat{y}_i$ is the prediction of the $i-th$ base learner, and W_i is the weight assigned to the $i-th$ base learner's prediction.

The weights W_i are often determined using cross-validation. The algorithm searches for the combination of weights that minimizes the overall prediction error, optimizing the ensemble's performance. The SLE method allows for flexibility and adaptability, as it can incorporate various base

learners and adjust their contributions based on their performance. This makes it a powerful tool for accurately predicting PQD and identifying the most influential features in the analysis.

Algorithm 2: Using SLE to identify for PQD signals

Input: fft_signals = a dataset (fft_result) containing features
class = pure(C1), sag(C2), swell(C3), oscillatory(C4), flicker(C5), harmonics(C6), interruption(C7), transient/impulse/spike(C8), notching(C9)
base_learners = kNN(L1), LR(L2), DT(L3), SVM(L4), GB(L5), AdaBoost(L6), RF(L7), ET(L8), NN(L9)

Parameters: n_estimators=10
n_splits=10

Output: ensemble_prediction
evaluate_acc

```
# Ensemble Creation and Training
 def super_learner_ensemble(fft_signals, class, base_learners):
  # Initialize an empty list from base learners
      predictions = [ ]
  # Loop over each base learner
      for learner in base_learners:
        learner.fit(fft_signals, class
  # Make predictions on the training data
      pred = learner.predict(fft_signals)
      predictions.append(pred)
  # Create a matrix with base learner predictions
  predictions_matrix = np.column_stack(predictions)
  # Initialize an array to store the weights
  weights = np.zeros(len(base_learners))

# Cross-Validation and Weight Calculation
  # Use cross-validation to determine the weights
  for i in range(len(base_learners)):
  # Exclude the i-th base learner from the ensemble
    sub_ensemble = np.delete(predictions_matrix, i, axis=1)
  # Train a meta-learner on the sub-ensemble
    meta_learner = MetaLearner()
    meta_learner.fit(sub_ensemble, class)
  # Calculate the weight for the i-th base learner
    weights[i] = meta_learner.coef_[i]
  # Normalize the weights to sum to 1
  weights /= np.sum(weights)

# Ensemble Prediction
  # Combine predictions of base learners
  ensemble_prediction = np.dot (predictions_matrix, weights)
  return ensemble_prediction

# Evaluate SLE using a performance metric
 # Accuracy
 evaluate_acc = accuracy(ensemble_prediction)
```

The acquired features were employed in the training of data using a SLE mechanism, specifically instantiated by a MetaLearner class. This MetaLearner class is instrumental in computing the weights assigned to baseline learners. It operates with three primary inputs: the FFT transform outcome, the PQD class designation, and a list of base learners. Through the utilization of cross-validation, the

weights associated with each baseline learner are ascertained and subsequently normalized to yield a cumulative sum of 1. This procedure culminates in the amalgamation of baseline learner predictions, incorporating their respective weights, which collectively furnish the resultant predictions. The final step entails the assessment of outcomes through performance metrics, encompassing accuracy. A brief depiction of these steps is summarized in algorithmic form within Algorithm 2 where nine base learners are used, namely k-nearest neighbors (KNN), logistic regression (LR), decision tree (DT), support vector machine (SVM), gradient boosting (GB), adaptive boosting (AdaBoost), random forest (RF), extra-trees (ET), and neural network (NN). The model fitting was accomplished through the utilization of the Python API within the Scikit-learn library, Numpy and Pandas for learning of classifier. [31]. The data input was split into a training set (2,025 sets:75%) and a testing set (675 sets:25%). Meanwhile, another data set from collecting actual (experimental) data was tested with 900 datasets (100 dataset per disturbance). The details of parameter settings used for computational experiments are shown in Table 5.

Table 5
Details on the computational settings used of classifier

Classifier	Parameters setting
KNeighbors	n_neighbors= 5
LogisticRegression	solver= liblinear
DecisionTree	criterion=gini
C-Support Vector	gamma=scale, probability=True
GaussianNB	var_smoothing=1e-09
AdaBoost	n_estimators=10
RandomForest	n_estimators=10
ExtraTrees	n_estimators=10
NeuralNetwork	activation = relu , L2 regularization
Super Learner Ensembles	n_splits=10, shuffle=True, n_samples_train=2,700, n_samples_test=900, centers=2, n_features=256, cluster_std=20

A schematic depiction of the proposed process is illustrated in Figure 5, comprising five principal stages:

i. Signal generation employing mathematical formulations;
ii. Normalization of individual datasets;
iii. FFT computation;
iv. Characterization of PQD utilizing SLE;
v. Empirical assessment of the model's performance through testing from Elec-meter data of PEA.

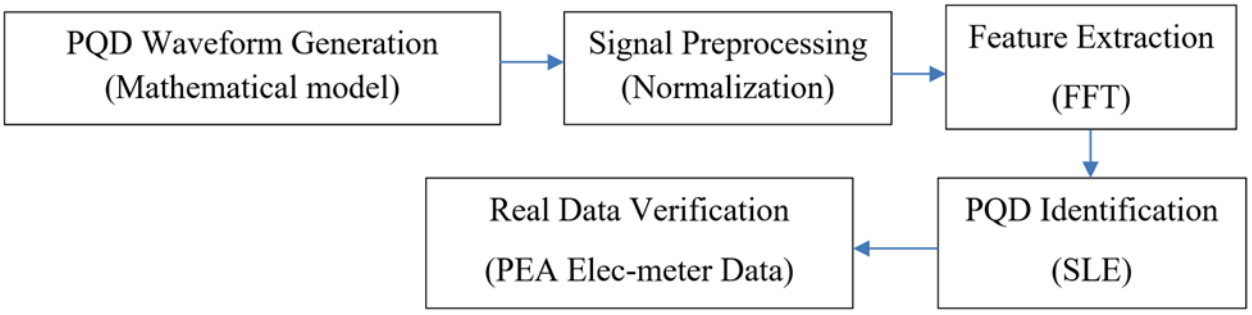

Fig. 5. Block diagram for the proposed method

3.2.4 Performance evaluation

Accuracy is a prevalent metric for assessing the effectiveness of classification models. This metric quantifies the percentage of correctly predicted labels, thereby measuring the overall success of the model's predictions [29]. The evaluation framework for accuracy is based on the interplay between key values denoted as TP (true positive), TN (true negative), FP (false positive), and FN (false negative), as elucidated by the following equation:

$$Accuracy = \frac{TP + TN}{TP + TN + FP + FN} \tag{8}$$

Within this evaluation, a confusion matrix is meticulously constructed with the overarching objective of discerning PQD events, encompassing a diverse matrix of 9 distinct classes. As an illustrative example, the process of computing the true positive rate and positive predictive rate for C7 is visually explained in Figure 6.

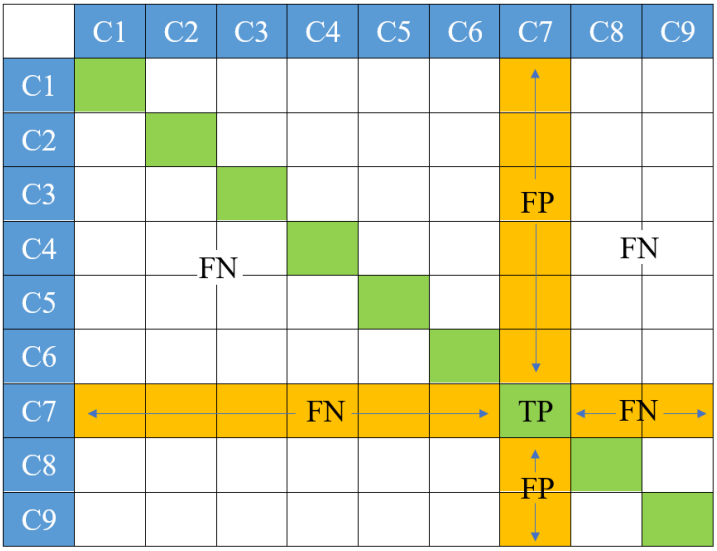

Fig. 6. Confusion matrix for 9 classes

4. Results and Discussion

Five subsections, namely classification results from synthetic data sets, validation of the method with experimental data sets, comparison with other recent publications, discussion, and limitations are presented in this section. The details of each subsection are as follows.

4.1 Classification Results from Synthetic Datasets

The transformed power spectrum is selected as an input to be utilized within the SLE model. The input data undergoes an iterative process across each base learner to predict values for the various classes outlined in the training. The output is presented in metric format. Importantly, the default weight value is maintained for each array, followed by the execution of cross-validation. This process involves the utilization of nine weights for each base learner: kNN, LR, DT, SVM, GB, AdaBoost, RF, ET, and NN, which employ default parameters. Subsequently, the weight values for each base learner are calculated and incorporated into SLE. The results of training and validation within the SLE

framework are depicted in Figure 7. Our data set was partitioned into 27 batch-sizes, each subjected to 100 iterations, where we set a total of 100 epochs. Remarkably, by the 20th iteration, both training and validation approaches exhibited remarkable accuracy, underscoring the model's proficiency in accurate prediction. Figure 8 showcases the validation outcomes for each base learner, evidencing the model's precise and comprehensive predictive ability, which in turn refines the weights and enhances the SLE's overall performance to its peak potential.

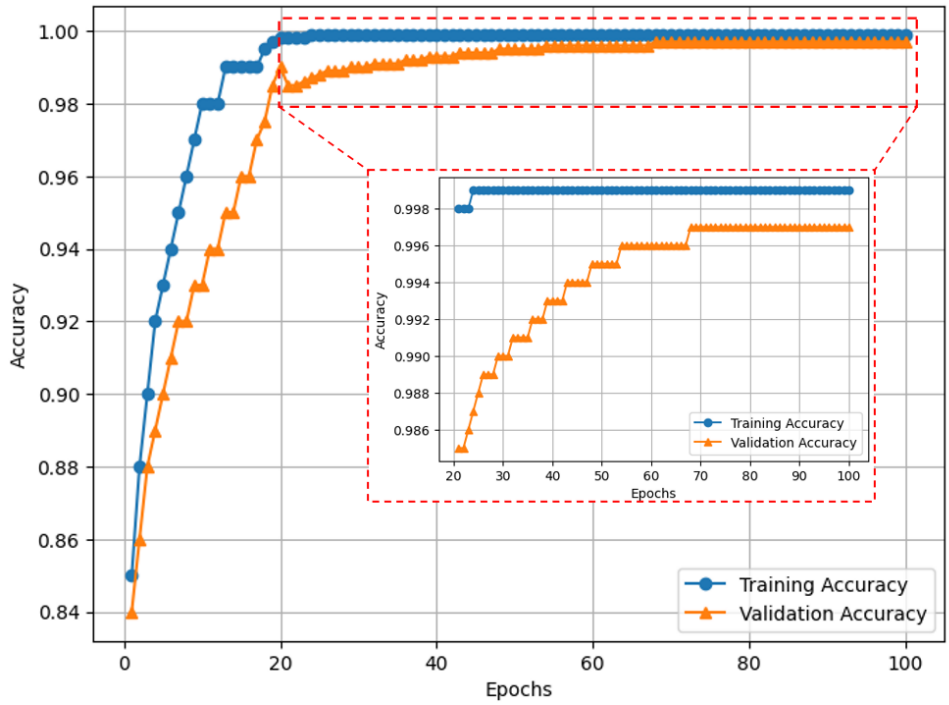

Fig. 7. Training and validation accuracy

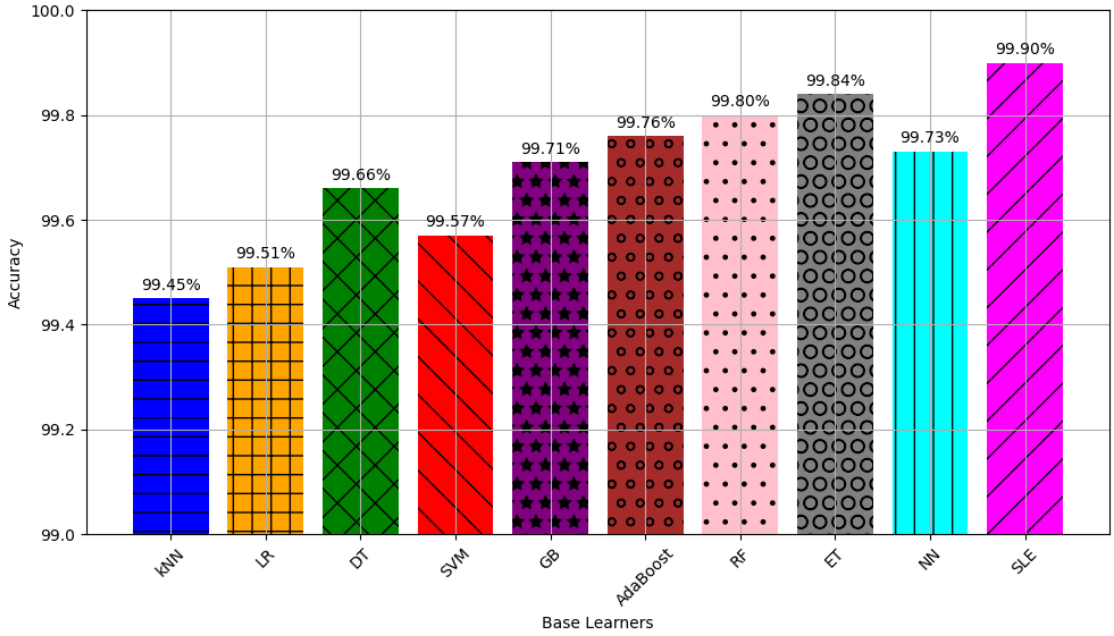

Fig. 8. Validation performance of base learners

4.2 Validation of the Method with Experimental Datasets

After analysing the training-validation outcomes, it was evident that the SLE model exhibited a commendable accuracy of 99.90%. Subsequently, the model was subjected to a distinct dataset derived from Elec-meters. Due to constraints posed by the meter's operational limits, a real-time characterization experiment was unfeasible. Consequently, the data was synthetically simulated in accordance with the specifications outlined in Table 3. The meter was programmed to display the corresponding real-time signals during this simulation. To elucidate, Figures 9 and 10 showcase captured signals: the upper figure depicts three-phase voltage, while the lower figure illustrates three-phase current values (with A-phase in red, B-phase in white, and C-phase in blue). These recorded values were stored and subsequently employed as inputs for the pre-established model.

In Figure 9, we simulate turn-on multiple air conditioners in a PEA office, leading to discernible changes in the signal that cause sag in A-phase and harmonics in C-phase current. Another case, Figure 10 demonstrates an occurrence of load switching at the Main Distribution Board (MDB), manifesting as oscillatory A-phase current and harmonics in the C-phase. The experiments conducted encompassed simulations of each of the nine PQD event types, facilitating comprehensive record-keeping of their respective occurrences.

Using the amassed data encompassing all distinct events, we input it into the model to make predictions concerning PQD characteristics. The accuracy of these predictions was subsequently assessed through an evaluation process involving a confusion matrix, as visually depicted in Figure 11. In this matrix, the diagonal (indicated by the green box) showcases the instances where the predicted outcomes align with the target values. Notably, for pure waveform events, the model exhibited an exceptionally high accuracy of 99.98%. However, for the flicker waveform, the predictions were comparatively less accurate, at 99.31%. The occurrences of mispredictions are represented within the orange box, reflecting instances where the model provided incorrect predictions. Upon closer examination, the flicker erroneously classified it as notching, with an error rate of 0.68%.

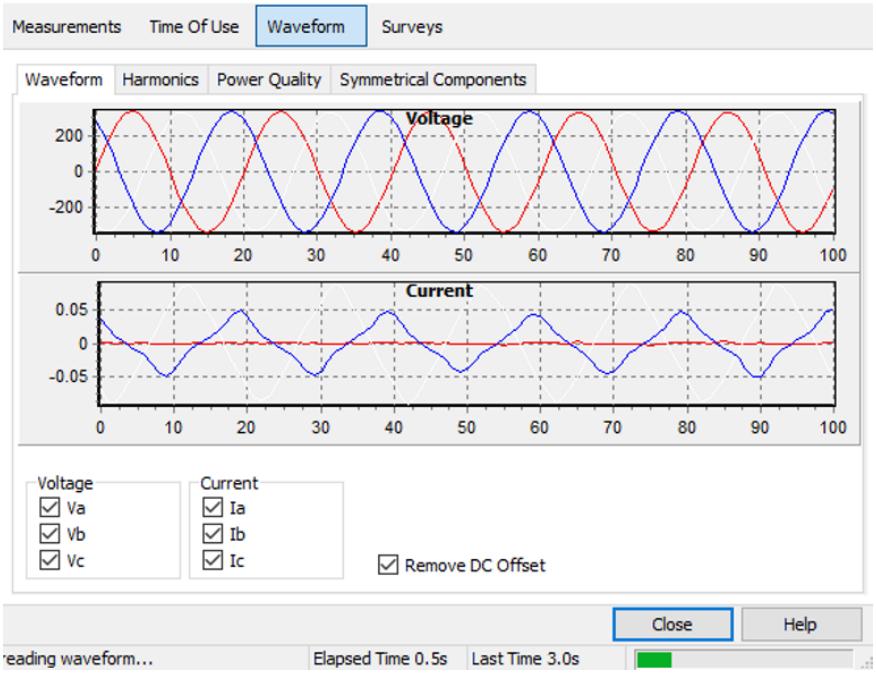

Fig. 9. Waveform read from Elec-meter (sag (Ia), harmonics(Ic))

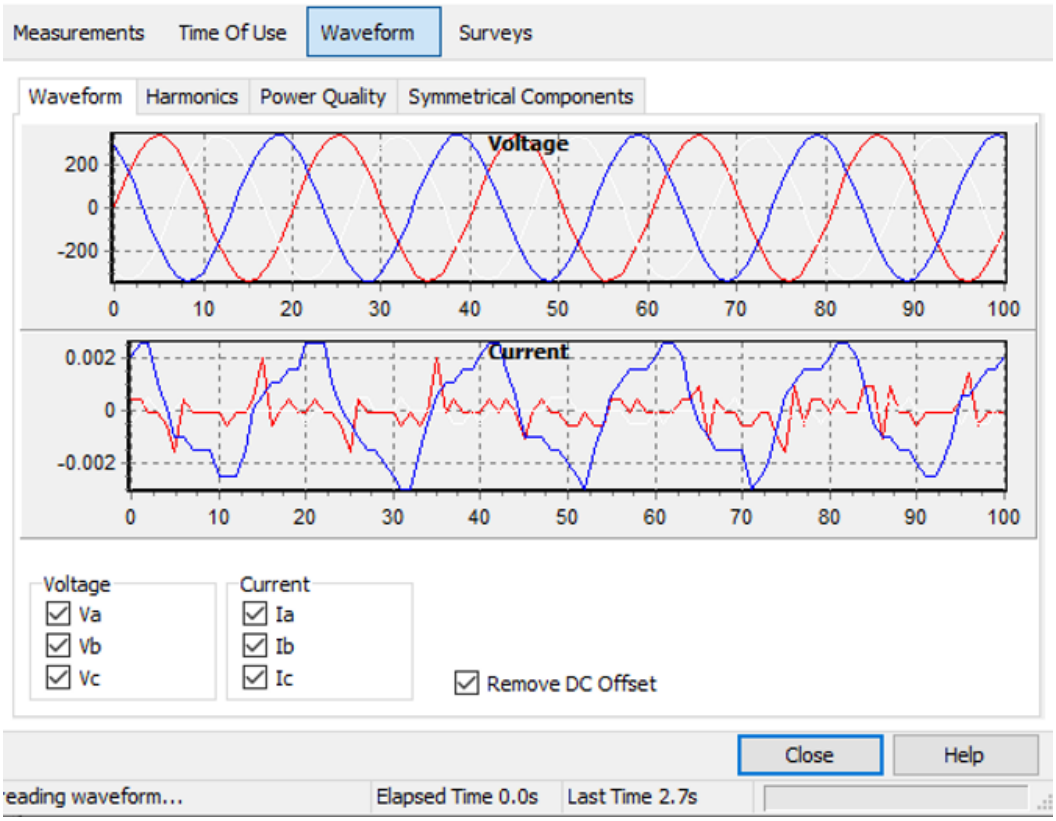

Fig. 10. Waveform read from Elec-meter (oscillatory (Ia), harmonics (Ic))

Predict Class	C1	C2	C3	C4	C5	C6	C7	C8	C9	
C1	99.98		0.01			0.01				99.98 0.02
C2		99.85		0.15						99.85 0.15
C3			99.79		0.2					99.79 0.2
C4		0.12		99.66		0.08		0.14		99.66 0.34
C5					99.31				0.68	99.31 0.68
C6	0.01			0.2		99.64			0.02	99.64 0.23
C7		0.03					99.82	0.15		99.82 0.18
C8			0.19					99.58		99.58 0.19
C9					0.5				99.47	99.47 0.5
	99.99 0.01	100 0.00	99.79 0.20	99.66 0.35	99.31 0.5	99.64 0.09	99.82 0.00	99.58 0.29	99.47 0.70	**99.69** **0.26**

Target Class

Fig. 11. Confusion matrix of testing dataset (% accuracy)

4.3 Comparison with Other Recent Publications

Table 6 provides a quantitative comparison between the proposed methodology and previously published approaches. This comparison encompasses various parameters, including event number, feature extraction, classification method, utilization of synthetic signals, and real signals for identification, to show the strengths of modelling and testing the model on real data.

Table 6
Performances comparison with other proposed methods

Reference	Event number	Feature extraction	Classification method	Accuracy (%) (Synthetic data)	Accuracy (%) (Real data)
(Shen *et al.,* 2017) [32]	8	CT	SVM	99.75	99.80
(Buduru *et al.,* 2023) [24]	5	HT	Fuzzy rules	99.27	97.17
(Amirou *et al.,* 2022) [33]	9	ST-CSK	XGboost	99.72	No
(Golla *et al.,* 2019) [34]	14	CWT	SVM	97.00	No
(Rodriguez *et al.,* 2021) [35]	9	HHT	LSTM-RNN	98.85	No
(Xu *et al.,* 2022) [36]	8	ADN	SVM	99.73	No
Proposed method	9	FFT	SLE	99.90	99.69

4.4 Discussion

In summary, the experimental findings, when considered with the conceptual framework depicted in Figure 5, have revealed four noteworthy insights. First, the observation pertains to the data generation process, which is grounded in a mathematical model, thereby endowing it with an idealization. While experimental instances employed randomized commands to generate PQD characteristic data, accounting for noise and incidental factors played a pivotal role in fostering the model's adaptability and versatility. Second, the insight emanates from the utilization of FFT for data extraction. Notably, the sequencing of $X[k]$ for k = 0,...,N-1 significantly influences the power spectrum, leading to more distinct plots. Third, the revelation centres around the modelling approach adopted for learning and validation through SLE. This technique harnesses the synergy of various conventional machine learning algorithms, amalgamating them into an ensemble that optimizes diverse learning algorithms. This collaborative strategy enhances the efficacy of the resulting model. Fourth, it pertains to the assessment of the model's performance using real data from Elec-meters. There are several limitations, such as the inability to conduct real-time testing, the necessity to simulate loads to store data, and dealing with relatively low data resolution. However, we are still able to test the functionality of the preliminary model.

In our discussion of the experimental outcomes, we have organized them into two distinct points for clarity. First, for the training and validation outcomes, as illustrated in Figure 7, a convergence in training accuracy is noticeable around the 25th iteration, while the validation accuracy converges around the 68th iteration, indicating a marginal disparity of 0.2%, underscoring the need for further refinement. When contrasting multiple traditional machine learning algorithms, a trend toward high accuracy becomes evident across various types. This range spans from a minimum of 99.45% in kNN to a maximum of 99.84% in ET. This diversity in accuracy can be attributed to the distinctive functionalities encoded within the algorithmic structures. For instance, parameters such as the number of neighbours (k) in kNN, the kernel function in SVM, and the count of trees in decision tree. In total, the integration of nine types plays a pivotal role in fine-tuning weights for SLE, thereby facilitating effective learning and predictive capabilities.

Second point of consideration, our examination of the model's performance against real data has discovered errors across all classes, as indicated in Figure 11. To illustrate, let's consider the example

of class C4 (oscillatory). The model correctly predicts instances of oscillatory events (TP) at a rate of 99.66%, while a minor fraction is misclassified as C2 (sag) or C6 (swell), contributing to FP at 0.15% and 0.2%, respectively. Conversely, instances where oscillatory events were missed (FN) including C2 at 0.12%, C6 at 0.08%, and C8 (transient) at 0.14%, amounting to a cumulative 0.34%. Notably, the consideration of TN is disregarded in scenarios where false predictions align with actual non-events.

The complex nature of PQD patterns gives rise to infrequent occurrences or instances where multiple patterns intersect. For instance, during periods of diminished waveform oscillations, the simultaneous manifestation of sag, swell, and oscillatory events may confound predictions. Furthermore, situations where transients are only partially captured by the meter contribute to prediction inaccuracies. These complexities collectively contribute to erroneous predictions by the model.

4.5 Limitations

In the above experiment, the results were satisfactory. However, there are still some issues that limit this experiment, including:

i. Real-time testing is not possible due to limitations in the capabilities of meters designed to focus on energy measurement and data acquisition.
ii. In some situations, the resulting PQD model is complex. Due to splitting multiple PQDs using FFT, which converts time-domain discrete signals into frequency-domain discrete spectra in this experiment, we are still unable to differentiate.

These limitations will be used as a guide for future research, and the results will be reported in the near future.

5. Conclusion

The increase in non-linear loads and the infiltration of renewable energy into the power system exacerbate power quality issues. This paper proposes a simple and efficient algorithm to identify nine types of single PQDs. The proposed algorithm consists of three main steps: (1) data normalization; (2) FFT-based feature extraction; and (3) classification with SLE. The resultant outcomes from data generated by mathematical equations are utilized for both training and validation within the SLE framework, culminating in a remarkable accuracy rate of 99.90%. This accuracy level significantly surpasses conventional machine learning methods. The developed algorithms are further subjected to evaluation using real-world data. Through the simulation of events and the recording of corresponding values via Elec-meters, the algorithms are thoroughly tested. The outcomes affirm the model's proficiency in accurately characterizing all nine types of PQDs with a high degree of precision.

For further study in the future, we plan to collect PQD data using a method that can capture more detailed values including the installation of equipment in the PEA system to collect events for analysis. Other research directions include the study of 1D, 2D, and 3D extraction methods and the application of deep learning for PQD classification, which is an interesting and popular technique nowadays.

Acknowledgments

This work was supported by the Faculty of Engineering, Academic Year 2023, Prince of Songkla University, Thailand, and in part by the Department of Electrical and Biomedical Engineering. The authors would like to thank the Meter and Transformer Section, Provincial Electricity Authority Ranot Branch, for providing simulated loads, profile retrieval, and event logs of simulation from Elec-meters.

References

[1] "IEEE Recommended Practice for Monitoring Electric Power Quality." In *IEEE Std 1159-2019 (Revision of IEEE Std 1159-2009)*, p. 1-98, 13 August 2019. https://doi.org/10.1109/IEEESTD.2019.8796486

[2] "Provincial Electricity Authority's Regulations on Electrical Network System Interconnection Code." In *PEA Std 2016*, p. 8 – 10.

[3] Provincial Electricity Authority. "PEA Customer Service (1129)." July 3, 2023.

[4] Norasonghi, Sakchai. "Power Quality." Accessed July 3, 2023.

[5] "IEEE Approved Draft Recommended Practice for Monitoring Electric Power Quality," In *IEEE P1159/D7, April 2019*, p. 1-104, 13 June 2019.

[6] Morsi, Walid G., and M. E. El-Hawary. "A new perspective for the IEEE standard 1459-2000 via stationary wavelet transform in the presence of nonstationary power quality disturbance." *IEEE Transactions on Power Delivery* 23, no. 4 (2008): 2356-2365. https://doi.org/10.1109/TPWRD.2008.2002660

[7] Khetarpal, Poras and Madan Mohan Tripathi. "A critical and comprehensive review on power quality disturbance detection and classification." *Sustainable Computing: Informatics and Systems* 28 (2020): 100417. https://doi.org/10.1016/j.suscom.2020.100417

[8] Saxena, Devesh Raj, Kshitij Verma and Subaran Singh. "Power quality event classification: an overview and key issues." *International journal of Engineering Science and Technology* 2 (2010): 186-199. https://doi.org/10.4314/ijest.v2i3.59190

[9] Liu, Huawu, Haibing Hu, Hao Chen, Li Zhang and Yan Xing. "Fast and Flexible Selective Harmonic Extraction Methods Based on the Generalized Discrete Fourier Transform." *IEEE Transactions on Power Electronics* 33 (2018): 3484-3496. https://doi.org/10.1109/TPEL.2017.2703138

[10] Dekhandji, Fatma Zohra. "Detection of power quality disturbances using discrete wavelet transform." In *Proceedings of 5th International Conference on Electrical Engineering - Boumerdes (ICEE-B), 2017.* 1-5. https://doi.org/10.1109/ICEE-B.2017.8192080

[11] Upadhyaya, S. and Sanjeeb Mohanty. 2013. "Power Quality disturbance detection using Wavelet based signal processing." In *Proceedings of Annual IEEE India Conference (INDICON), 2013.* 1-6. https://doi.org/10.1109/INDCON.2013.6725992.

[12] Kumar, Raj, Bhim Singh, D. T. Shahani, Ambrish Chandra and Kamal Al-haddad. "Recognition of Power-Quality Disturbances Using S-Transform-Based ANN Classifier and Rule-Based Decision Tree." *IEEE Transactions on Industry Applications* 51 (2015): 1249-1258. https://doi.org/10.1109/TIA.2014.2356639

[13] Yao, Wenxuan, Qiu Tang, Zhaosheng Teng, Yunpeng Gao and He Wen. "Fast S-Transform for Time-Varying Voltage Flicker Analysis." *IEEE Transactions on Instrumentation and Measurement* 63 (2014): 72-79. https://doi.org/10.1109/TIM.2013.2277618.

[14] Shamachurn, Heman. "Assessing the performance of a modified S-transform with probabilistic neural network, support vector machine and nearest neighbour classifiers for single and multiple power quality disturbances identification." *Neural Computing and Applications* 31 (2019): 1041-1060. https://doi.org/10.1007/s00521-017-3136-z

[15] Mahela, Om Prakash, Baseem Khan, Hassan Haes Alhelou and Sudeep Tanwar. "Assessment of power quality in the utility grid integrated with wind energy generation." *IET Power Electronics* (2020): n. pag. https://doi.org/10.1049/iet-pel.2019.1351

[16] Tse, Norman Chung-Fai, John Y. C. Chan, Wing-hong Lau and Loi Lei Lai. "Hybrid Wavelet and Hilbert Transform With Frequency-Shifting Decomposition for Power Quality Analysis." *IEEE Transactions on Instrumentation and Measurement* 61 (2012): 3225-3233. https://doi.org/10.1109/TIM.2012.2211474

[17] Afroni, Mohammad Jasa, Danny Sutanto and David Stirling. "Analysis of Nonstationary Power-Quality Waveforms Using Iterative Hilbert Huang Transform and SAX Algorithm." *IEEE Transactions on Power Delivery* 28 (2013): 2134-2144. https://doi.org/10.1109/TPWRD.2013.2264948

[18] Sahani, Mrutyunjaya and Pradipta Kishore Dash. "Automatic Power Quality Events Recognition Based on Hilbert Huang Transform and Weighted Bidirectional Extreme Learning Machine." *IEEE Transactions on Industrial Informatics* 14 (2018): 3849-3858. https://doi.org/10.1109/TII.2018.2803042

[19] Hemapriya, C. K., M. V. Suganyadevi and C. K. Krishnakumar. "Detection and classification of multi-complex power quality events in a smart grid using Hilbert–Huang transform and support vector machine." *Electrical Engineering* (2020): 1-26. https://doi.org/10.1007/s00202-020-00987-8
[20] Li, Jianmin, Zhaosheng Teng, Qiu Tang and Junhao Song. "Detection and Classification of Power Quality Disturbances Using Double Resolution S-Transform and DAG-SVMs." *IEEE Transactions on Instrumentation and Measurement* 65 (2016): 2302-2312. https://doi.org/10.1109/TIM.2016.2578518
[21] Mian Qaisar, Saeed, Nehal Alyamani, Asad Waqar and Moez Krichen. "Machine Learning with Adaptive Rate Processing for Power Quality Disturbances Identification." *SN Computer Science* 3 (2021): 1-6 https://doi.org/10.1007/s42979-021-00904-1
[22] Akbarpour, Amin, Mehdi Nafar and Mohsen Simab. "Multiple power quality disturbances detection and classification with fluctuations of amplitude and decision tree algorithm." *Electrical Engineering* (2022): 1-11. https://doi.org/10.1007/s00202-021-01481-5
[23] Zhu, Kunzhi, Zhaosheng Teng, Wei Qiu, Qiu Tang and Wenxuan Yao. "Complex Disturbances Identification: A Novel PQDs Decomposition and Modeling Method." *IEEE Transactions on Industrial Electronics* 70 (2023): 6356-6365. https://doi.org/10.1109/TIE.2022.3194575
[24] Buduru, Naveen Kumar and Srinivas Bhaskar Karanki. "Real-Time Power Quality Event Monitoring System Using Digital Signal Processor for Smart Metering Applications." *Journal of Electrical Engineering and Technology* 18 (2023): 3179 - 3190. https://doi.org/10.1007/s42835-023-01413-2
[25] Igual, Raúl, Carlos Medrano, Francisco Javier Arcega and Gabriela Măntescu. "Integral mathematical model of power quality disturbances." In *Proceedings of 18th International Conference on Harmonics and Quality of Power (ICHQP)*, 2018, 1-6. https://doi.org/10.1109/ICHQP.2018.8378902
[26] George, Timothy A. and David Bones. "Harmonic power flow determination using the fast Fourier transform." *IEEE Power Engineering Review* 6 no. 2 (1991): 530-535. https://doi.org/10.1109/61.131107
[27] van der Laan, Mark J., Eric C. Polley and Alan E. Hubbard. "Super Learner." *Statistical Applications in Genetics and Molecular Biology* 6, no. 1 (2007).
[28] Provincial Electricity Authority, "Provincial Electricity Authority Regulations on the Practice of Meters 2019." Last modified July 10, 2023.
[29] Karasu, Seçkin and Zehra Saraç. "Investigation of power quality disturbances by using 2D discrete orthonormal S-transform, machine learning and multi-objective evolutionary algorithms." *Swarm and Evolutionary Computation* 44 (2019): 1060-1072. https://doi.org/10.1016/j.swevo.2018.11.002
[30] SciPy Documentation. "Fourier Transforms (scipy.fft)." Accessed July 10, 2023. https://docs.scipy.org/doc/scipy/tutorial/fft.html.
[31] scikit-learn. "Machine Learning in Python, Ensemble Methods." Accessed July 10, 2023.
[32] Shen, Yue, Fida Hussain, Hui Liu and Destaw Addis. "Power quality disturbances classification based on curvelet transform." *International Journal of Computers and Applications* 40 (2017): 192-201. https://doi.org/10.1080/1206212X.2017.1398213
[33] Amirou, Ahmed, Yanis Amirou and Djaffar Ould-Abdeslam. "S-Transform with a Compact Support Kernel and Classification Models Based Power Quality Recognition." *Journal of Electrical Engineering and Technology* 17 (2022): 2061 - 2070. https://doi.org/10.1007/s42835-022-01009-2
[34] Golla, Mallikarjuna and Kumar Chandrasekaran. "Cross Wavelet-SVM for Detection and Classification of Power Quality Problems in Distribution System." In *Proceedings of the International Conference on Power Electronics Applications and Technology in Present Energy Scenario (PETPES), 2019,* 1-5. https://doi.org/10.1109/PETPES47060.2019.9003772
[35] Rodriguez, Miguel Angel, John Felipe Sotomonte, Jenny Alexandra Cifuentes and Maximiliano Bueno-López. "A Classification Method for Power-Quality Disturbances Using Hilbert–Huang Transform and LSTM Recurrent Neural Networks." *Journal of Electrical Engineering and Technology* 16 (2020): 249-266. https://doi.org/10.1007/s42835-020-00612-5
[36] Xu, Yanchun, Shi-shuai Fan, Shasha Xie and Mi Lu. "Power Quality Detection and Classification in Active Distribution Networks Based on Improved Empirical Wavelet Transform and Dispersion Entropy." *CSEE Journal of Power and Energy Systems* 8, no. 6 (2022). https://doi.org/10.17775/CSEEJPES.2020.00110